www.sciencemag.org/cgi/content/full/science.aat0271/DC1

Supplementary Materials for

Programming self-organizing multicellular structures with synthetic cell-cell signaling

Satoshi Toda, Lucas R. Blauch, Sindy K. Y. Tang, Leonardo Morsut*, Wendell A. Lim*

*Corresponding author. Email: leonardo.morsut@med.usc.edu (L.M.); wendell.lim@ucsf.edu (W.A.L.)

Published 31 May 2018 on *Science* First Release
DOI: 10.1126/science.aat0271

This PDF file includes:

Other Supplementary Materials for this manuscript include the following:
(available at www.sciencemag.org/cgi/content/full/science.aat0271/DC1)

Materials and Methods

synNotch Receptor and Response Element Construct Design

synNotch receptors were built by fusing the CD19 scFv(*40*), LaG17 GFP nanobody(*41*) to the mouse Notch1 (NM_008714) minimal regulatory region (Ile1427 to Arg1752) and Gal4-VP64 or TetR-VP64 (tTA). All synNotch receptors contain an n-terminal CD8a signal peptide (MALPVTALLLPLALLLHAARP) for membrane targeting and a myc-tag (EQKLISEEDL) for LaG17 synNotch or HA-tag (YPYDVPDYA) for anti-CD19 synNotch to detect surface expression with anti-myc Alexa647 (cell-signaling #2233) or anti-HA-Alexa647 (Cell Signaling #3444). The receptors were cloned into a modified pHR'SIN:CSW vector containing EF1a promoter or SFFV promoter. The pHR'SIN:CSW vector was also modified to make the response element plasmids. Five copies of the Gal4 DBD target sequence (GGAGCACTGTCCTCCGAACG) or seven copies of the tetracycline responsive element (TRE, TCCCTATCAGTGATAGAGA) were cloned 5' to a minimal CMV promoter. Ecad was amplified from the plasmid gifted from the Keith Mostov lab. Ncad was amplified from the plasmid gifted from the Joshua A.Weiner lab. Pcad was amplified from the plasmid pβact-Pcad [BCCM/LMBP #2766]. CD19-P2A-BFP (CD19 connected with BFP by P2A sequence) and Pcad-IRES-mCherry (Pcad connected with mCherry by IRES sequence) were cloned into a MCS downstream of the EF1a promoter. CD19 was cloned into a MCS downstream of the SFFV promoter. Ecad, GFPlig, Ecad fused with mCherry at C-terminus, Ncad-P2A-GFPlig, mCherry-P2A-Pcad were cloned into a MCS downstream of the TRE inducible promoter. Ecad and TetR-KRAB (tTS)-P2A-GFP were cloned into a MCS downstream of the UAS inducible promoter. All constructs were cloned via Infusion cloning (Clontech #ST0345)).

Cell Lines

L929 mouse fibroblast cells (ATCC# CCL-1) were cultured in DMEM (invitrogen) containing 10% fetal bovine serum (University of California, San Francisco [UCSF] Cell Culture Facility) with penicillin and streptomycin. K562s were lentivirally transduced to stably express CD19 ligand or GFPlig. All cell lines were sorted for expression of the transgenes. All cell cultures were maintained in an incubator at 37 °C with 5% CO_2 and humidity.

Engineering of L929 cells with synNotch circuits

We established single-cell clonal populations which express a synNotch receptor to induce cadherin to minimize a dispersion of cadherin induction amount in the population. For lentiviral transduction, 5x10^4 or 1x10^5 of L929 cells were plated in 24-well or 12-well plates respectively. 4 - 400 μl of viral supernatant was added to infect cells in the presence of 4 μg/ml polybrene. Two or three days after infection, the cells were split into two wells, and the cells in one well were stimulated with K562 expressing CD19 ligand or GFPlig next day. After 24hr co-culture with the K562 cells, the cells that were activated to express fluorescence protein or Ecad were sorted into 96 well plate at a single cell per well via a cell sorter FacsAriaII or Aria Fusion (Beckton-Dickinson). Ecad expression was measured by staining with anti-Ecadherin-PECy7 (BioLegend #147309). We screened clones by measuring the basal/induced expression amount of fluorescence proteins and cadherins. We picked up several clones which have low basal but high induction of target genes and then tested them in a spheroid culture. To check the induction of Ecad and fluorescence proteins in the three-layer circuit in Fig. S2A, 10000 cells of each cell type were plated in 96well. Next day 4x10^4 K562 cells expressing CD19 ligand or GFPlig was added. After 24hr incubation, cells were stained with anti-Ecad-PECy7 and analyzed with FACS

Aria fusion. To label the A-type cells in a top panel of Fig. S1A, we used CellTrace Far Red (Invitrogen #C34564). To label the B-type cells in Fig. 2, we transduced them with a histone H2B fused with infrared fluorescent protein (H2B-IFP) as a nuclear marker.

Spheroid assay

We plated a defined number of engineered L929 cells in 96-well round-bottom ultra-low-attachment plate (Corning #7007) to form a spheroid. After plating cells in each well, we spin the plate down at 100xg for 2 min and incubated it at 37 °C with 5% CO_2 and humidity. In Fig. 4 and Fig. S5, we used FACS Aria Fusion to sort 100 cells into each well. To inhibit synNotch signaling, we added 25 μM DAPT (TOCRIS #2634) in media.

Microscopy

Images and movies were taken on a microscope with a custom built environmental chamber with temperature and CO_2 control (In Vivo Scientific) on a Nikon Eclipse Ti inverted microscope equipped with a Yokogawa spinning disk confocal (CSU-W1), a 20x PlanFluor 0.75 NA objective or 10x PlanApo 0.45 NA objective, and an electron microscopy charge-coupled device (EM-CCD) camera (Photometrix). 405 nm, 488 nm, 561 nm, and 640 nm laser wavelengths (LMM5, Spectral Applied Research) were used for excitation. For typical experiments, we observed 4-8 replicates of each condition. For time lapse imaging, we imaged every 15 or 30min for 24 to 50hr. MicroManager software was used to design the imaging protocols and collect the actual data. ImageJ macro was used to apply the conditions of contrast and brightness to all samples in each experiment and output the images and movies.

Building a composite circuit of lateral inhibition and cell sorting for two-layer formation from single genotype

First we established the cell line which undergoes cell type bifurcation by lateral inhibition circuit with synNotch receptor. To measure how much repressor tTS expression is required to repress CD19 ligand expression, L929 was lentivirally transduced with CD19-P2A-mCherry expressed by TetO promoter (CMV promoter with 2x TRE binding sites) and tTS-P2A-GFP expressed by SV40 promoter. Fig. S4A shows that around 200 A.U. GFP intensity was enough to repress mCherry expression. Based on this result, we established multiple clones of L929 which express anti-CD19 synNotch Gal4VP64 receptor inducing tTS-P2A-GFP via UAS promoter with a low GFP background (<100 A.U.) but high GFP induction (>>200 A.U.). Then we introduced TetO driving CD19-P2A-mCherry in these clones and established multiple clones which show cell type bifurcation into two populations of mCherry-high/GFP-low and mCherry-low/GFP-high (Fig. S4B). To induce self-driven two layer formation from single cell type, we transduced UAS promoter controlling Ecadherin in the lateral inhibition clone we established above. Finally, we established multiple clones which show two populations of mCherry-high/GFP-low/Ecad-negative and mCherry-low/GFP-high/Ecad-positive. To shut off the lateral inhibition circuit by inhibiting synNotch signaling, we cultured cells in the presence of 25 μM DAPT for a week in Fig. 4D and Fig. S5C.

Regeneration assay

In order to demonstrate the robustness of our designed system to physical perturbations, we bisected our spheroids using a microfluidic guillotine previously developed to bisect single cells to study cellular regeneration(*18*). We plated 160 A-type cells and 80 B-type cells in the three-

layer circuit in Fig. 2D. We checked the three-layer structure formation after 24hr incubation, cut the structure with the microfluidic guillotine next day, and observed the regeneration of the cleaved structures for 25 hours. For bisecting spheroids, we adjusted the channel geometry and cutting velocity. The dimensions of the channel were chosen based on two criteria. 1) The channel should be sufficiently small to confine the spheroid within the channel so that the centroid of the spheroid was aligned to the knife for reproducible bisection into two equal halves. 2) The confinement should be just sufficient to avoid excessive shear on the spheroid at the channel wall. We tested different channel cross-section size (130 μm x 50 μm, 150 μm x 50 μm and 200 μm x 50 μm (width x height)) and found 150 μm x 50 μm led to sufficient confinement of the spheroid in the channel while reducing the damage to the spheroid by shear. We injected the spheroids at a flow rate of 148 cm/s. At flow rates lower than this value, the organoids were not able to consistently enter the channel. We note that this flow rate was about 200 times higher than that required to cut Stentor coeruleus(*18*), likely due to the increased stiffness of the spheroids compared with Stentor.

Supplementary figure 1. Two layer formation requires Ecadherin induction and synNotch signaling

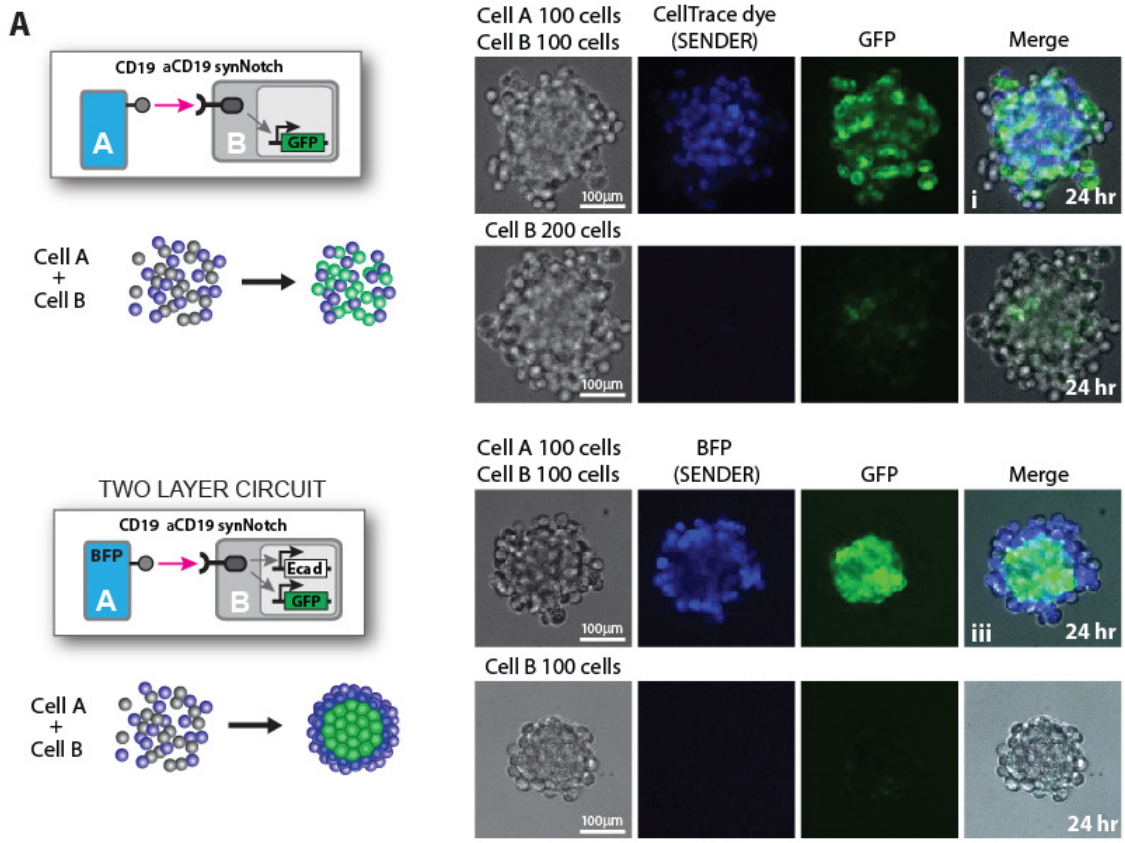

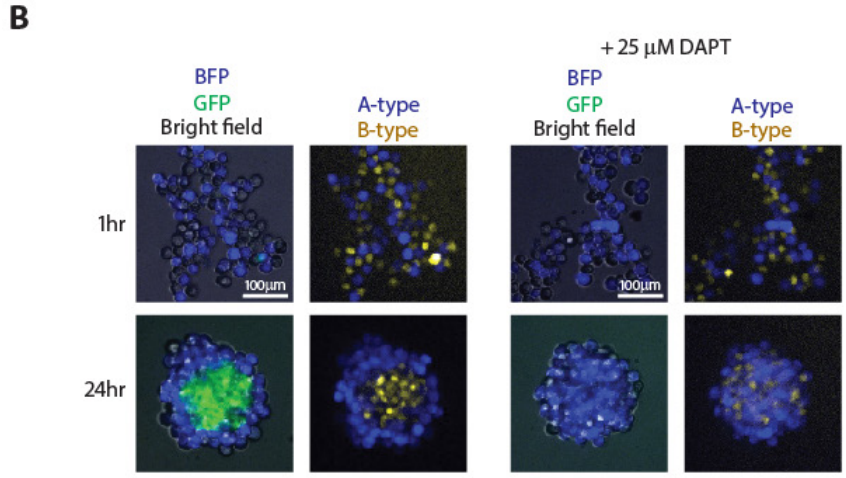

Fig. S1. Two layer formation requires Ecadherin induction and synNotch signaling

(A) Images of the spheroids driven by Two-layer circuit with or without Ecadherin at 24hr. A-type sender cell expressing CD19 ligand induces GFP (top) or Ecad and GFP (bottom) in B-type receiver cell. In the top circuit, B-type cells were activated to express GFP for 24hr incubation, but the A-type and B-type cells were randomly mixed without spatial organization. When Ecad and GFP were induced in B-type cells, the two-layer structure of Ecad-induced green inner core and blue loose outer layer was formed. Without A-type sender cells, B-type receiver cells expressed no GFP and formed a loose aggregate in both circuits.

(B) Disruption of two-layer formation by inhibiting synNotcn signaling with DAPT. Images of the spheroid starting with 100 A-type cells and 100 B-type cells at 1hr and 24hr were shown. A merge image of blue A-type cells (BFP) and yellow B-type cells (yellow indicates H2B-IFP expressed in the B-type cells) shows the distribution of A-type and B-type cells. The two-layer structure was formed at 24hr without DAPT and B-type cells were localized in an inner core. On the other hand, in the presence of 25 μM DAPT, GFP and Ecad were not induced in the B-type cells, resulting the A-type and B-type cells were randomly distributed.

Supplementary Figure 2. Building a three-layer formation circuit by two step signaling inducing a high and low level of Ecadherin

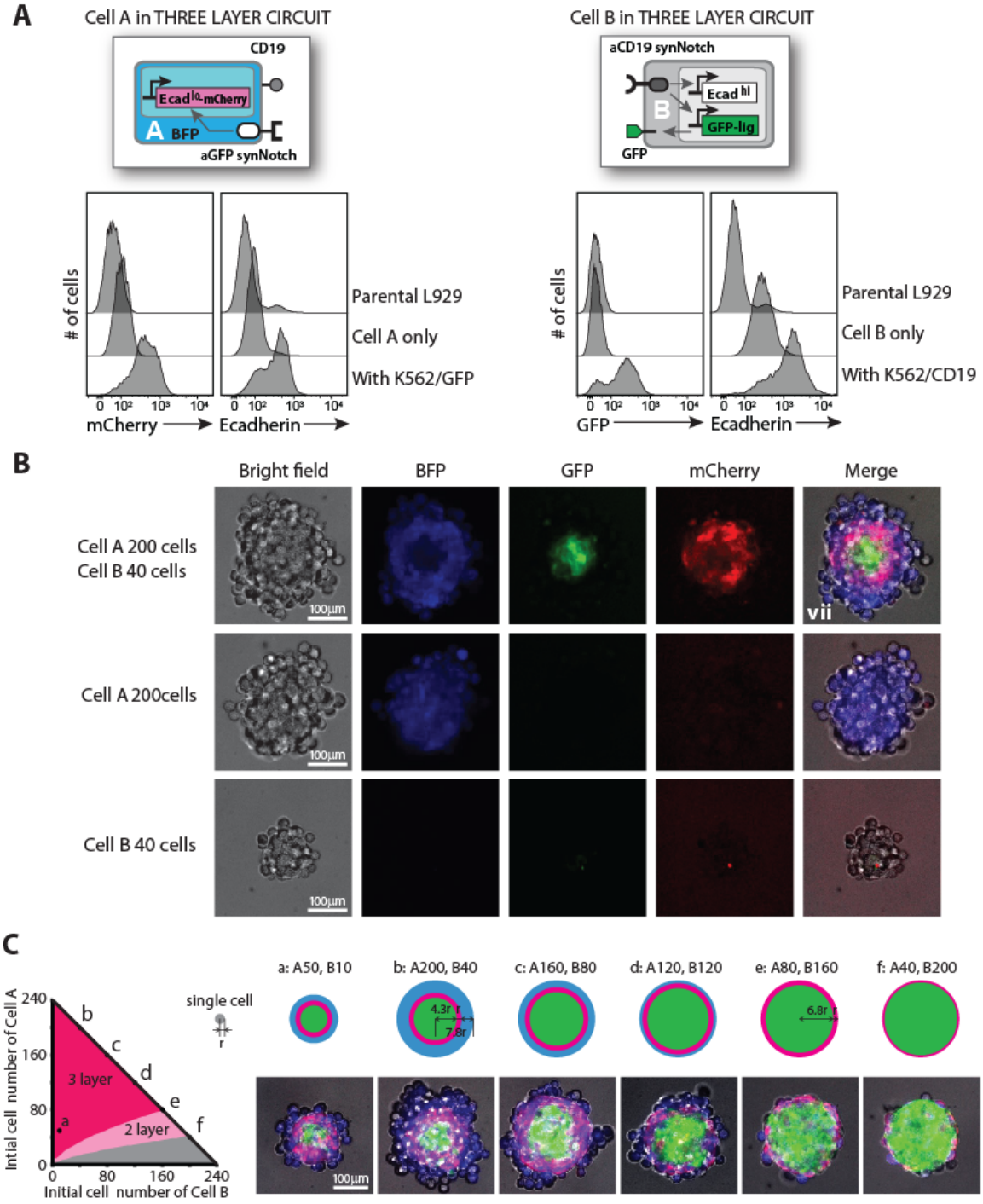

Fig. S2. Building a three-layer formation circuit by two step signaling inducing a high and low amount of Ecadherin

(A) Establishment of Cell A and Cell B in the three-layer circuit. The Cell A expresses BFP, CD19 ligand and anti-GFP synNotch inducing a low amount of Ecadherin fused with mCherry (Ecadlo-mCherry). We stimulated A-type cells with K562 expressing GFPlig and confirmed the induction of mCherry and Ecadlo (~500 A.U.). The right panel shows the Cell B expresses anti-CD19 synNotch inducing a high amount of Ecadherin (Ecadhi) and GFPlig. We stimulated B-type cells with K562 expressing CD19 ligand and confirmed the induction of GFPlig and Ecadhi (~2000 A.U.). B-type cells have a background Ecad expression without stimulation compared to parental L929, but this leaky Ecad expression was not enough to induce tight compaction (Fig. S2B) and cell sorting (Fig. S3B).

(B) Images of each fluorescence channel of three-layer structure starting with 200 A-type cells and 40 B-type cells at 24hr. A spheroid of only A-type cells showed no mCherry induction and little compaction by Ecad. A spheroid of only B-type cells showed no GFP induction and little compaction by leaky Ecad.

(C) Robust three-layer formation to the initial cell number/ratio of A-type and B-type cells. We changed the initial cell number/ratio of A-type cells and B-type cells to see how much the initial cell number/ratio influences the output structure. In the left graph, we predicted the output structure by calculating radius of each layer in a spheroid based on the initial cell number/ratio. Here, we set "r" as a radius of a cell and postulate that the number of total cells increases twice after 24hr culture because L929 undergoes cell division once per about 24hr. When we co-culture 200 A-type cells and 40 B-type cells (condition b), the final total cell number will be 480 and the radius of the spheroid and green inner core will be $\sqrt[3]{480}\cdot r$ (~7.8r) and $\sqrt[3]{80}\cdot r$ (~4.3r), respectively. We also postulate that the width of red layer is approximate to r because red cell shape becomes flat to be adhesive on the green core. Therefore, the green core is expected to be located at a range of 0~4.3r, red layer at 4.3r~5.3r and blue layer at 5.3r~7.8r. We did similar calculations for all conditions of different initial number of A and B-type cells in the left graph, including condition a to f (top Images). In the case of 80 A-type cells and 160 B-type cells, the spheroid radius is $\sqrt[3]{480}\cdot r$ (~7.8r) and the green core radius is and $\sqrt[3]{320}\cdot r$ (~6.8r), so all A-type cells located at a range of 6.8r~7.8r will be in a red layer (condition e). We calculated a threshold line between three and two layer in the left graph at the ratio in which all the A-type cells are located in the red layer. If B-type cells increase more, the layer of A-type cells become thinner, so we set a threshold line of two-layer structure at the ratio in which A-type cells form the red layer with a half width of r. We co-cultured the A-type and B-type cells at the conditions of a-f and observed their spheroids (bottom images). These spheroids showed similar structures to the predicted structures (top images).

Supplementary Figure 3. Three-layer formation requires Ecadherin induction and synNotch signaling

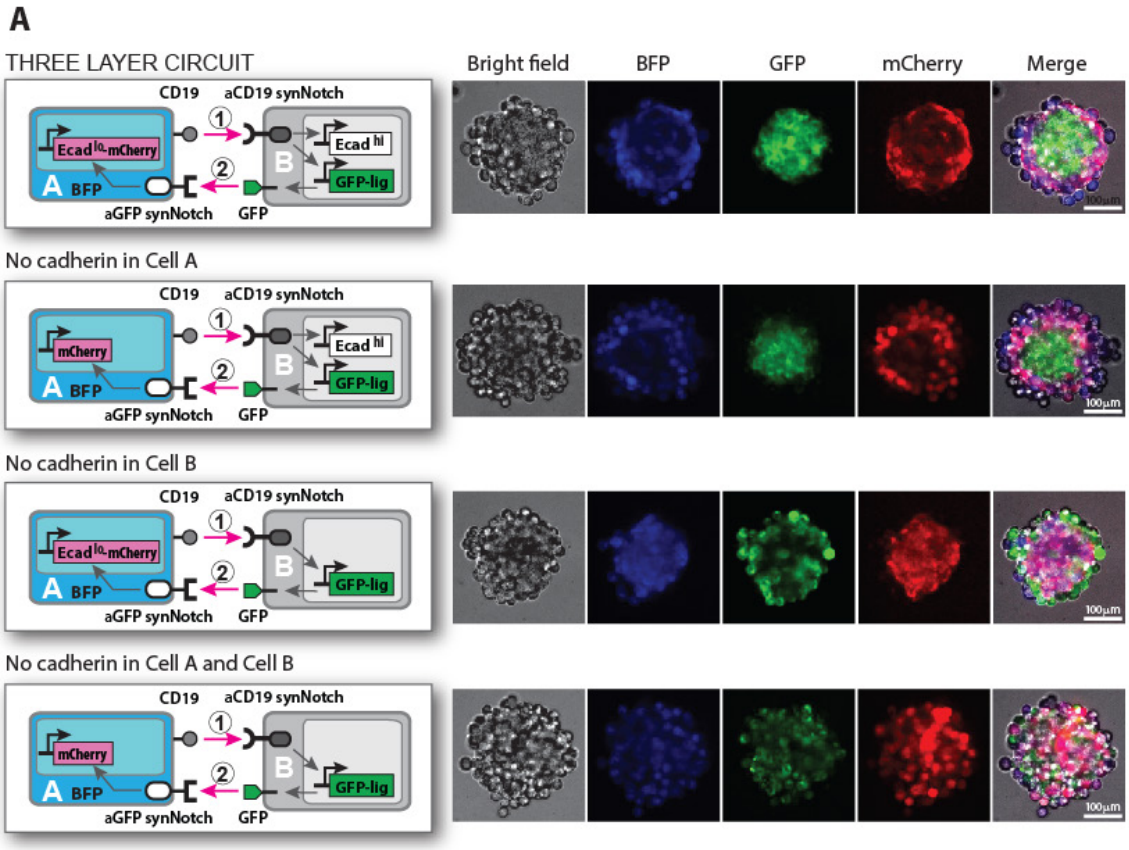

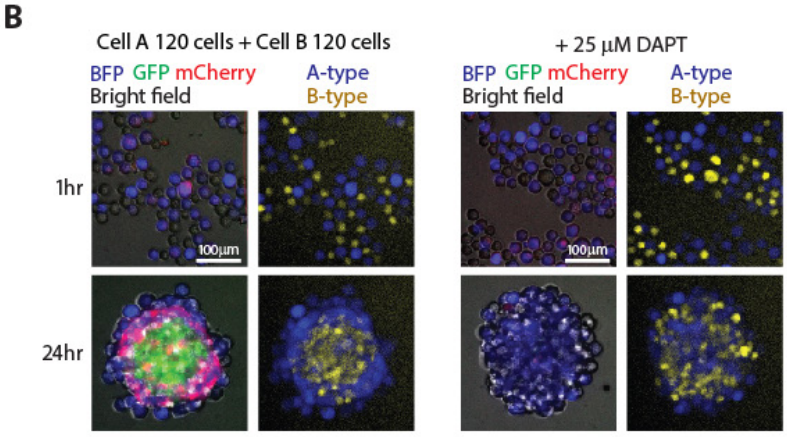

Fig. S3. Three-layer formation requires Ecadherin induction and synNotch signaling

(A) Three-layer circuit with or without Ecadherin. The first pannel shows the three-layer circuit and structure as shown in Fig. 2. In the case of no cadherin in Cell A (second pannel), the first signaling by CD19 induces Ecadhi and GFPlig in B-type cells to form a green inner core. Then, the second signaling by induced GFPlig activated mCherry in A-type cells attaching the green core. As a result, the structure was close to the three layer, but the no-Ecad red cells did not bind to green core tightly, so the border between blue and red layer was loose. In the case of no cadherin in Cell B (third pannel), the first signaling induces GFPlig in B-type cells without cell sorting. Then, the second signaling activated Ecadlo and mCherry in A-type cells, leading to the red core formation of activated A-type cells. Most of no-Ecad green B-type cells were sorted out to the outer layer, though a low amount of Ecad in A-type cells were not enough to sort all B-type cells out. In the case of no cadherin in both Cell A and Cell B (fourth pannel), the first signaling induces GFPlig in B-type cells without cell sorting, and then the second signaling activated mCherry in A-type cells. As a result, the structure was a random mixture of activated A-type and B-type cells. Without Ecadherin induction, only synNotch signaling could not increase cell type and form spatially-organized structure.

(B) Disruption of three-layer formation by inhibiting synNotch signaling with DAPT. Images of the spheroid starting with 120 A-type cells and 120 B-type cells at 1hr and 24hr were shown. A merge image of blue A-type cells (BFP) and yellow B-type cells (yellow indicates H2B-IFP expressed in the B-type cells) shows the distribution of each cell type. Without DAPT, the three-layer structure was formed at 24hr and B-type cells were sorted inside to form a green inner core. On the other hand, in the presence of 25 μM DAPT, GFPlig, Ecadhi, and Ecadlo-mCherry were not induced in the B-type and A-type cells respectively, and the distribution of the A-type cells and B-type cells showed no cell sorting occurred.

Supplementary figure 4. Building the lateral inhibition circuit with synNotch

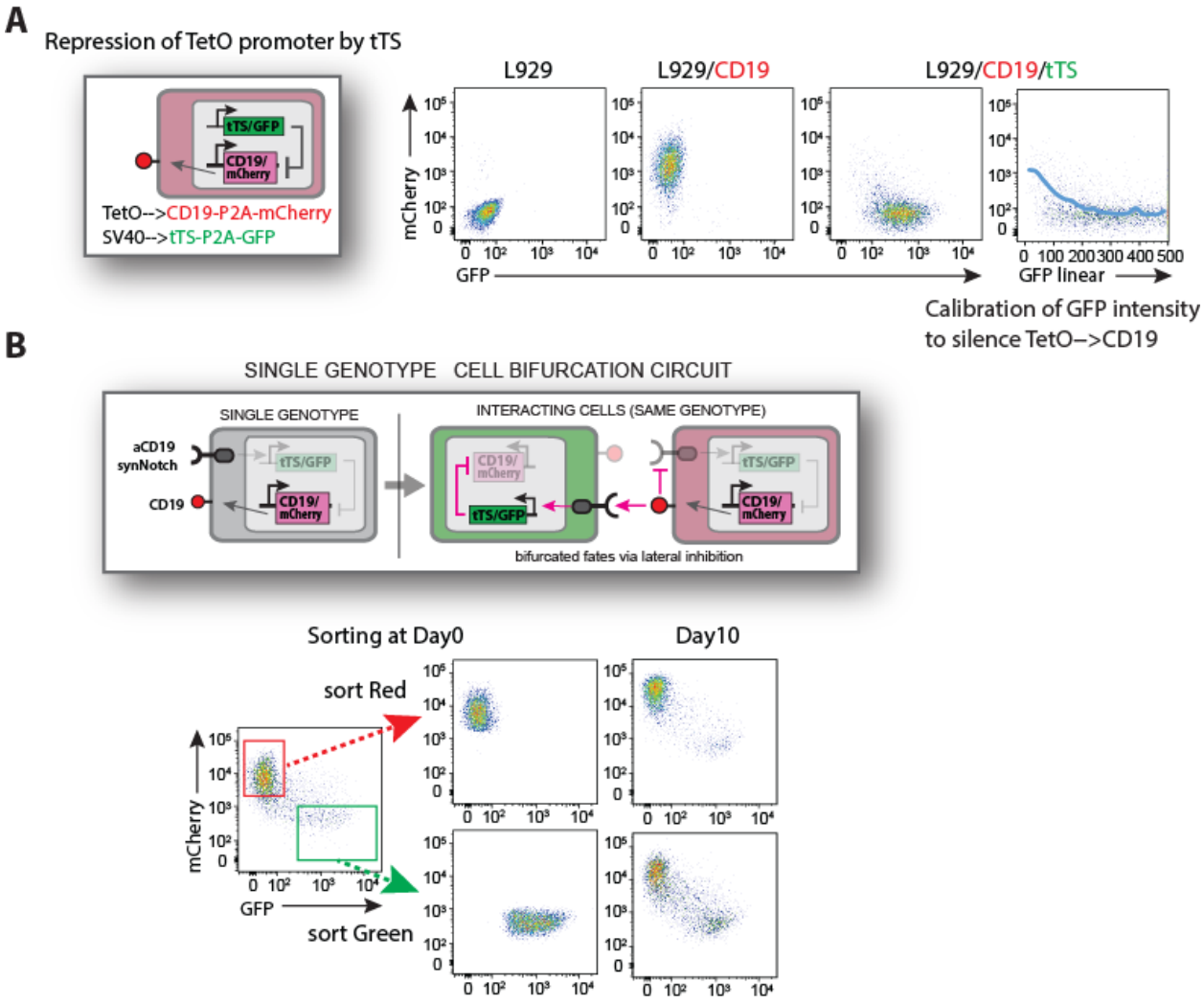

Fig. S4. Building the lateral inhibition circuit with synNotch

(A) Calibration of how much tTS is required to repress TetO promoter driving CD19. L929 cells were lenti-virally transduced with TetO driving CD19-P2A-mCherry and SV40 driving tTS-P2A-GFP. We analyzed mCherry and GFP fluorescence intensity of L929, L929/TetO→CD19-P2A-mCherry (L929/CD19) and L929/TetO→CD19-P2A-mCherry/SV40→tTS-P2A-GFP (L929/CD19/tTS) at day 9 after infection. In the far right plot, we overlay a plot of mean mCherry intensity over every 25 A.U. of the GFP intensity. About 100-200 A.U. of GFP was enough to repress mCherry signal, suggesting that the leaky expression of GFP should be < 100 A.U. and induced GFP intensity should be >> 200 A.U. to build the lateral inhibition circuit.

(B) Cell fate bifurcation with the lateral inhibition circuit using synNotch. We transduced L929 cells to express CD19 and anti-CD19 synNotch which induces a repressor tTS and GFP to repress CD19 and mCherry expression. The mutual transcriptional repression of CD19 between adjacent cells can amplify a small initial difference of CD19 amount between cells, resulting in bimodal cell states of CD19/mCherry-high cells or tTS/GFP-high cells. A representative distribution of mCherry-high or GFP-high cells that grew from a single cell clone was shown in the bottom left plot. We purified mCherry-high or GFP-high cells by cell sorting and observed that both purified populations robustly regenerated two cell populations of mCherry-high or GFP-high.

Supplementary figure 5. Two layer formation from single genotype population by the lateral inhibition circuit inducing Ecadherin-positive and negative populations

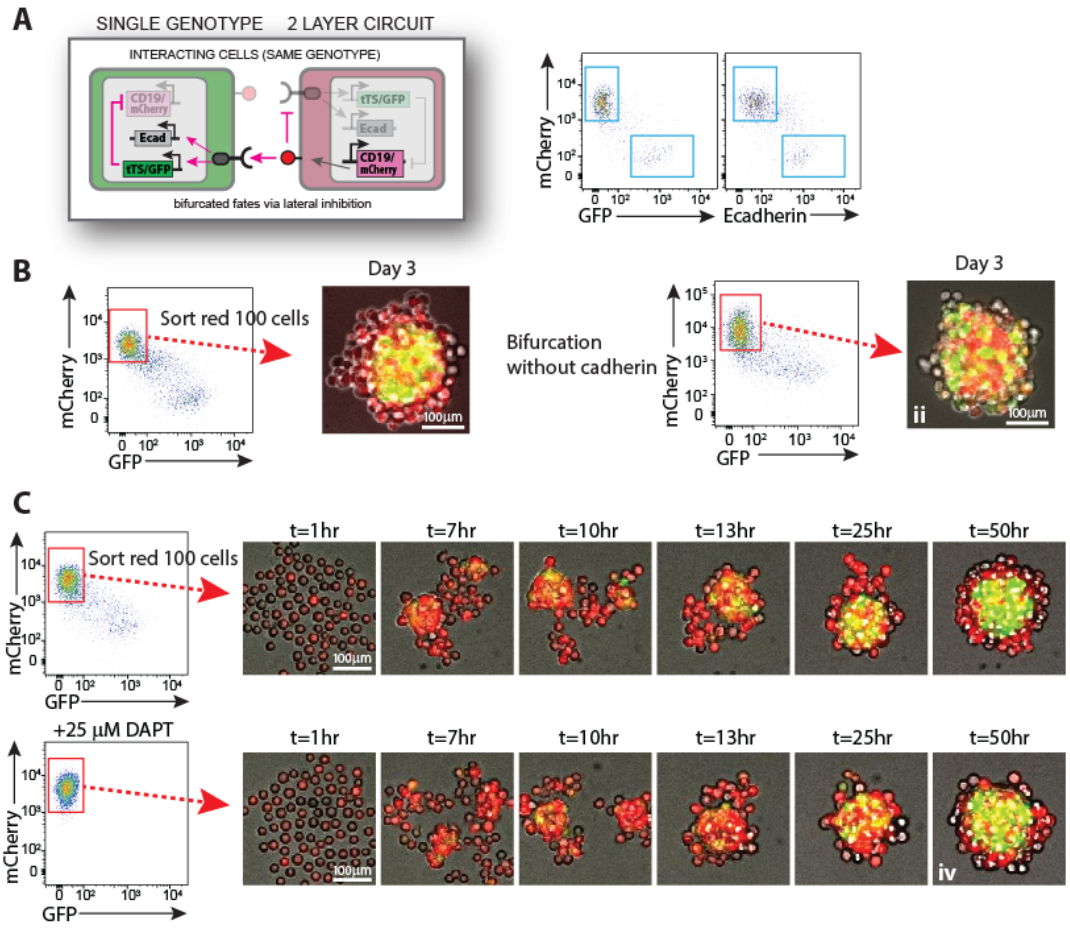

Fig. S5. Two-layer formation from single genotype population by the lateral inhibition circuit inducing Ecadherin-positive and negative populations

(A) Building the lateral inhibition circuit inducing Ecad-positive and negative populations from single genotype. We introduced Ecad with the synNotch-driven promoter in the lateral inhibition circuit. The right plots show a representative clone that bifurcates into two populations: CD19/mCherry-high or tTS/GFP/Ecad-high.

(B) Two-layer formation from single cell type. We purified 100 mCherry-high cells expressing the lateral inhibition circuit with or without Ecad induction to culture them in a spheroid. After 3-day incubation, mCherry-high cells expressing the lateral inhibition circuit inducing Ecad underwent bifurcation into mCherry-high or GFP/Ecad-high populations, resulting in two-layer formation (left pannel). On the other hand, mCherry-positive cells expressing the lateral inhibition circuit without Ecadherin underwent bifurcation and formed a checker board-pattern of mCherry-high and GFP-high populations (right pannel).

(C) The time course of two-layer formation from single cell type. The top row shows sorted 100 mCherry-positive cells underwent bifurcation and some populations became GFP/Ecad-high to be sorted inside and form a green inner core. Finally, two-layer structure was formed. In the bottom row, cells were cultured in the presence of 25 μM DAPT for a week to shut off synNotch signaling. As a result, GFP-high cells were cleared, confirming that the cell type bifurcation depends on synNotch signaling. Then we placed 100 mCherry-high cells to culture them in a spheroid in the absence of DAPT to initialize cell-cell signaling. These cells started signaling again and could re-bifurcate into mCherry-high or GFP/Ecad-high populations to form the two-layer structure.

Supplementary figure 6. Phase separation of Pcadherin-expressing sender cells and receiver cells inducing Ncadherin

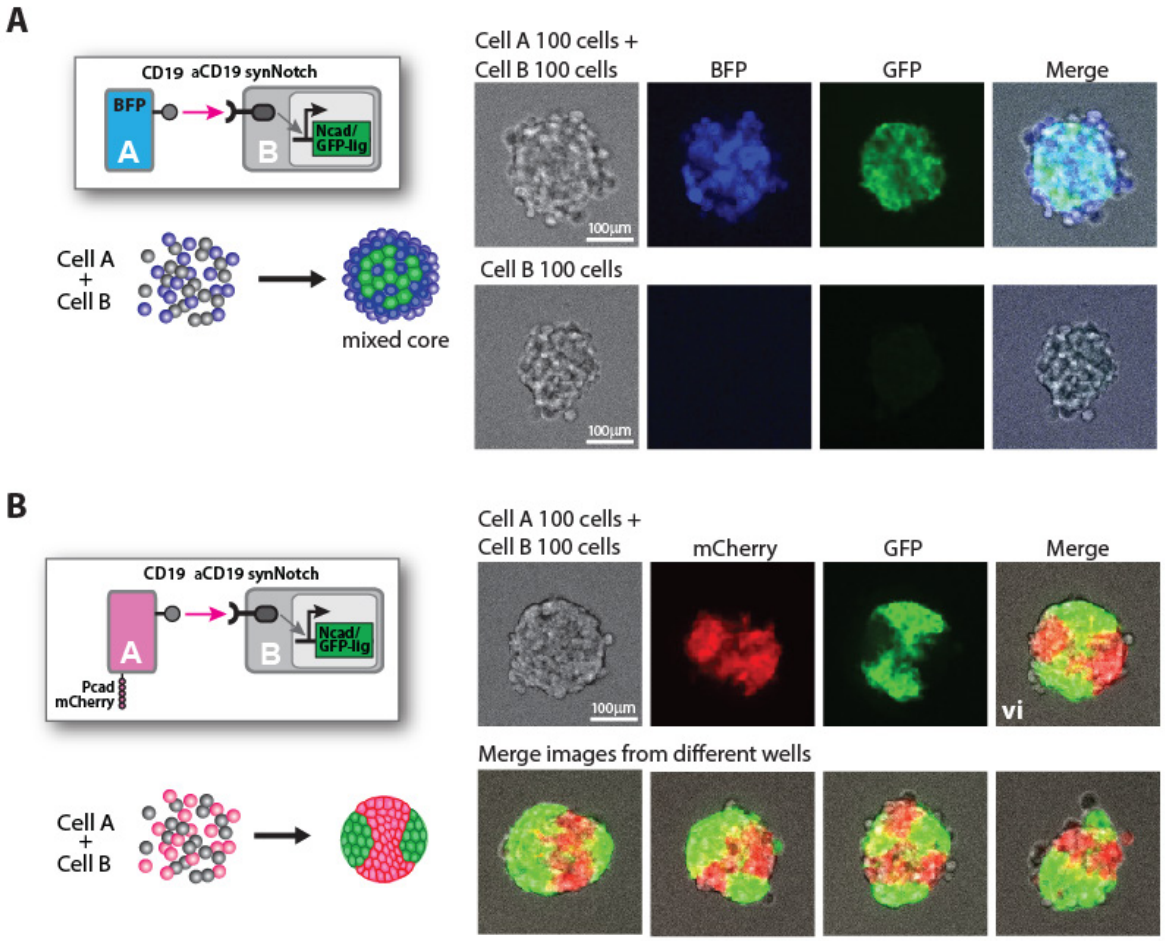

Fig. S6. Phase separation of Pcadherin-expressing sender cells and receiver cells inducing Ncadherin

(A) We tested spatial organization by Ncad induction in the two-layer circuit. We co-cultured CD19-expressing sender cells with receiver cells that express anti-CD19 synNotch inducing Ncad and GFPlig. After co-incubation, B-type cells became Ncad and GFP-positive to form a central core, but A-type cells were not well sorted out, suggesting that Ncad has a weaker ability to induce distinct regions of Ncad-positive or negative poplations by itself in L929 spheroids. A spheroid of only B-type cells showed no induction of GFP without A-type cells.

(B) Phase separation of Pcad-expressing sender cells and receiver cells inducing Ncad in two-layer circuit. When CD19-expressing sender cells expressed Pcad constitutively in the same circuit as above, Pcad-positive A-type cells and Ncad-induced B-type cells were well segregated to form distinct regions of each cell type. Similar segregation of red and green regions was observed in other replicate wells.

Supplementary Figure 7. Asymmetric three-layer formation with three-layer circuit inducing Ncadherin and Pcadherin.

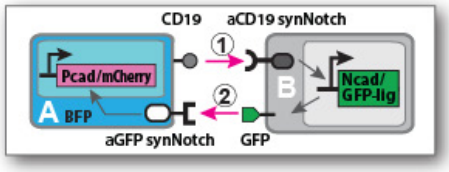

THREE LAYER
ASYMMETRIC
CIRCUIT (I)

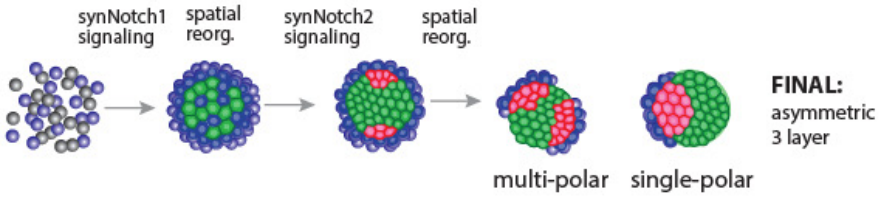

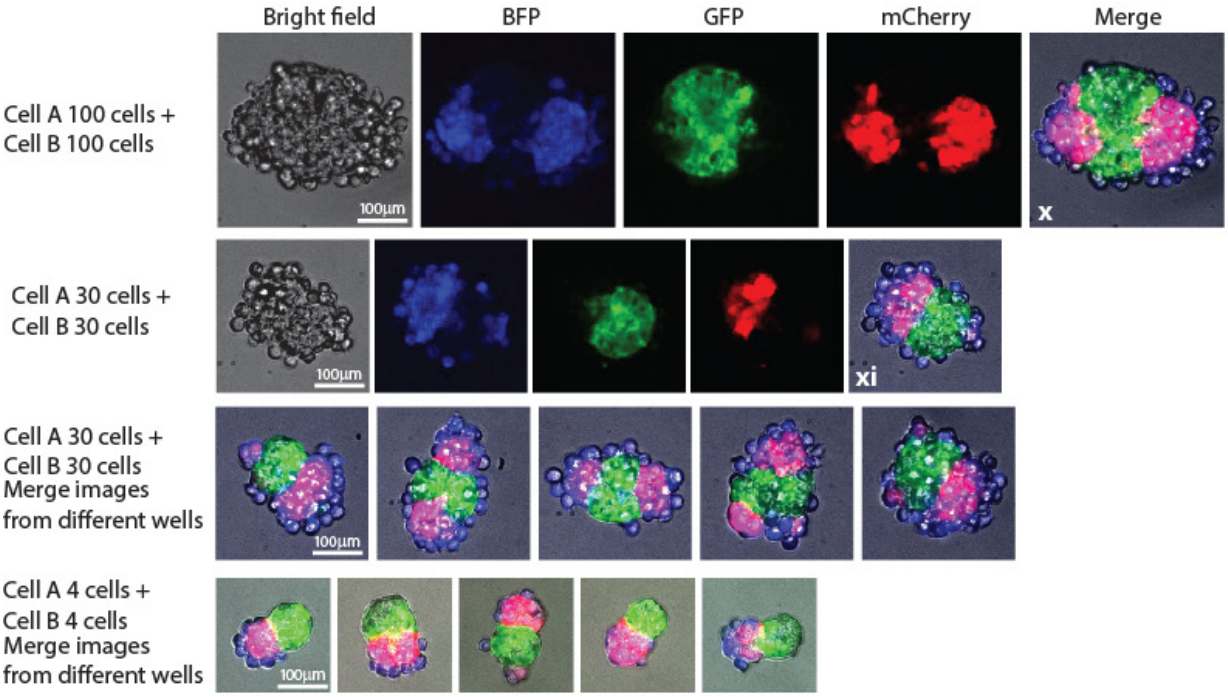

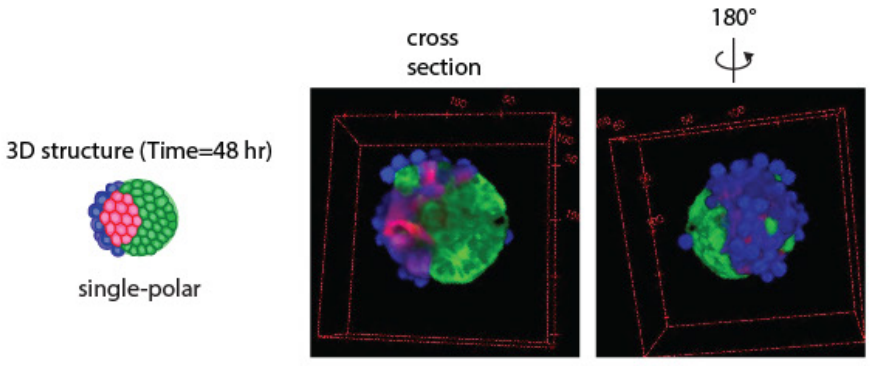

Fig. S7. Asymmetric three-layer formation with three-layer circuit inducing Ncadherin and Pcadherin.

We show images of asymmetric three-layer structure at 50hr starting with 100 or 30 of A-type and B-type cells in the three-layer asymmetric circuit (I) in Fig. 5B. In this circuit, first, Ncad and GFPlig were induced in B-type cells to form a green core, and then A-type cells attaching B-type cells were activated to express Pcad and mCherry, leading to self-segregation of green and red regions to form multiple red poles. Some blue A-type cells were located on the red poles and not activated through their anti-GFP synNotch, resulting in non-concentric three-layer formation. We also show many replicates of the spheroids starting with 30 cells of each cell type at 50hr and the spheroids with 4 cells of each cell type at 72hr. We found a smaller spheroid could form not only two-polar three-layer structure but also a single polar structure frequently likely because its small size limits surface area to initiate pole formation. 3D reconstruction image of the asymmetric three layer with a single pole of red cells was shown in the bottom. See Movie S4 for timelapse videos and 3D reconstruction.

Supplementary figure 8. Asymmetric three-layer formation with two step signaling inducing phase separation and boundary layer formation

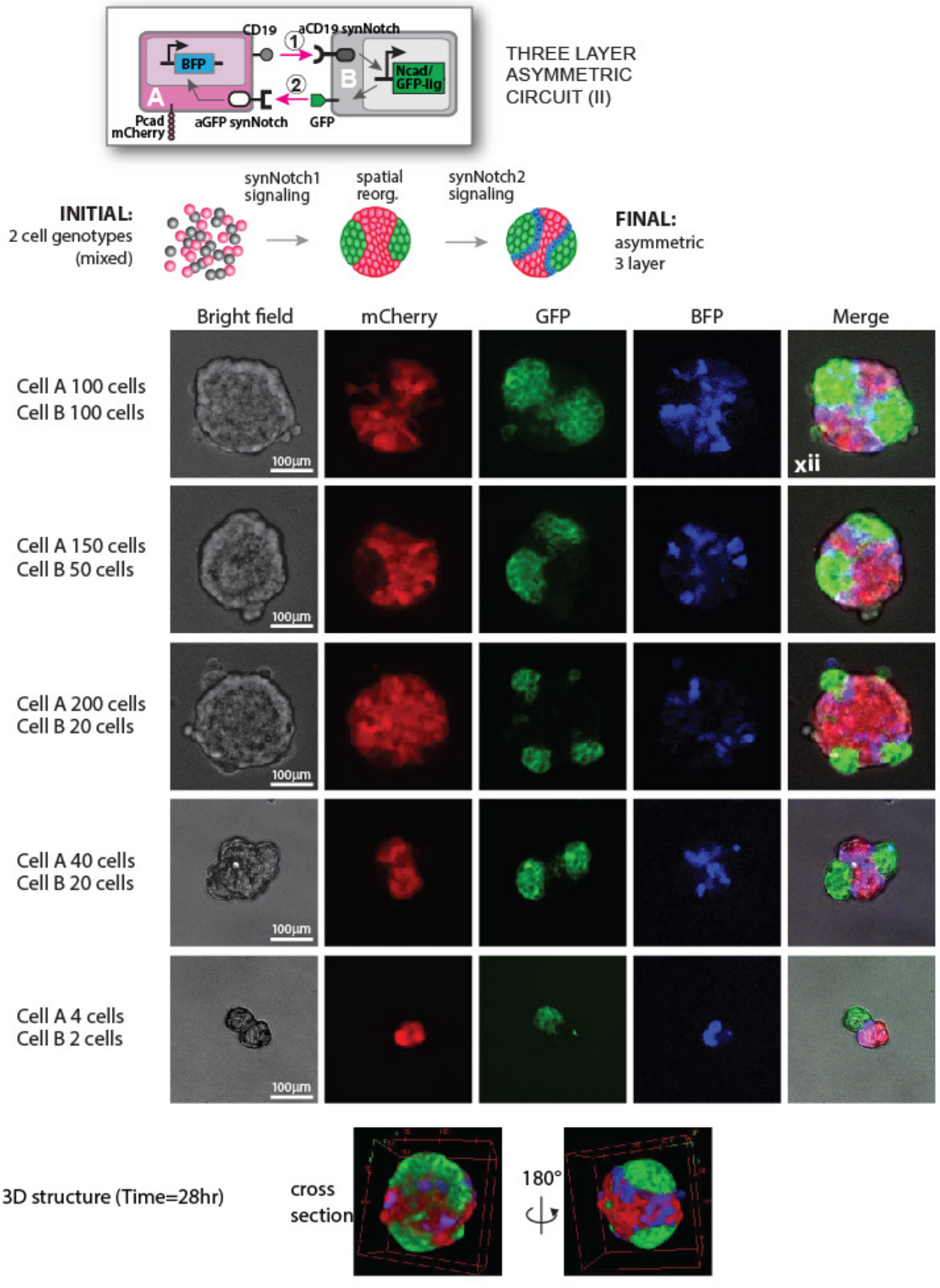

Fig. S8. Asymmetric three-layer formation with two step signaling inducing phase separation and boundary layer formation.

We show images starting from a different number of cells in the three-layer asymmetric circuit (II) in Fig. 5C. In this circuit, Pcad-expressing A-type cells induced Ncad and GFPlig in B-type cells, leading to their self-segregation to form B-type cells' polarized protrusions. Then, A-type cells at the boundary with B-type cells were activated by induced GFPlig to turn on BFP, resulting in blue boundary layer formation between the polarized green and red regions. Asymmetric three-layer structure was formed in 24hr with step-wise induction of phase separation and boundary layer formation robustly to initial cell number/ratio of each cell type. The smallest spheroid (starting with Cell A 4 cells and Cell B 2 cells) was imaged at 48hr. At the bottom, 3D reconstruction images starting with 160 A-type cells and 80 B-type cells at 28hr were shown. See Movie S5 for timelapse video and 3D reconstruction.

Supplementary Figure 9. Spherically symmetric three-layer formation with three-layer circuit inducing Ecadherin and Pcadherin.

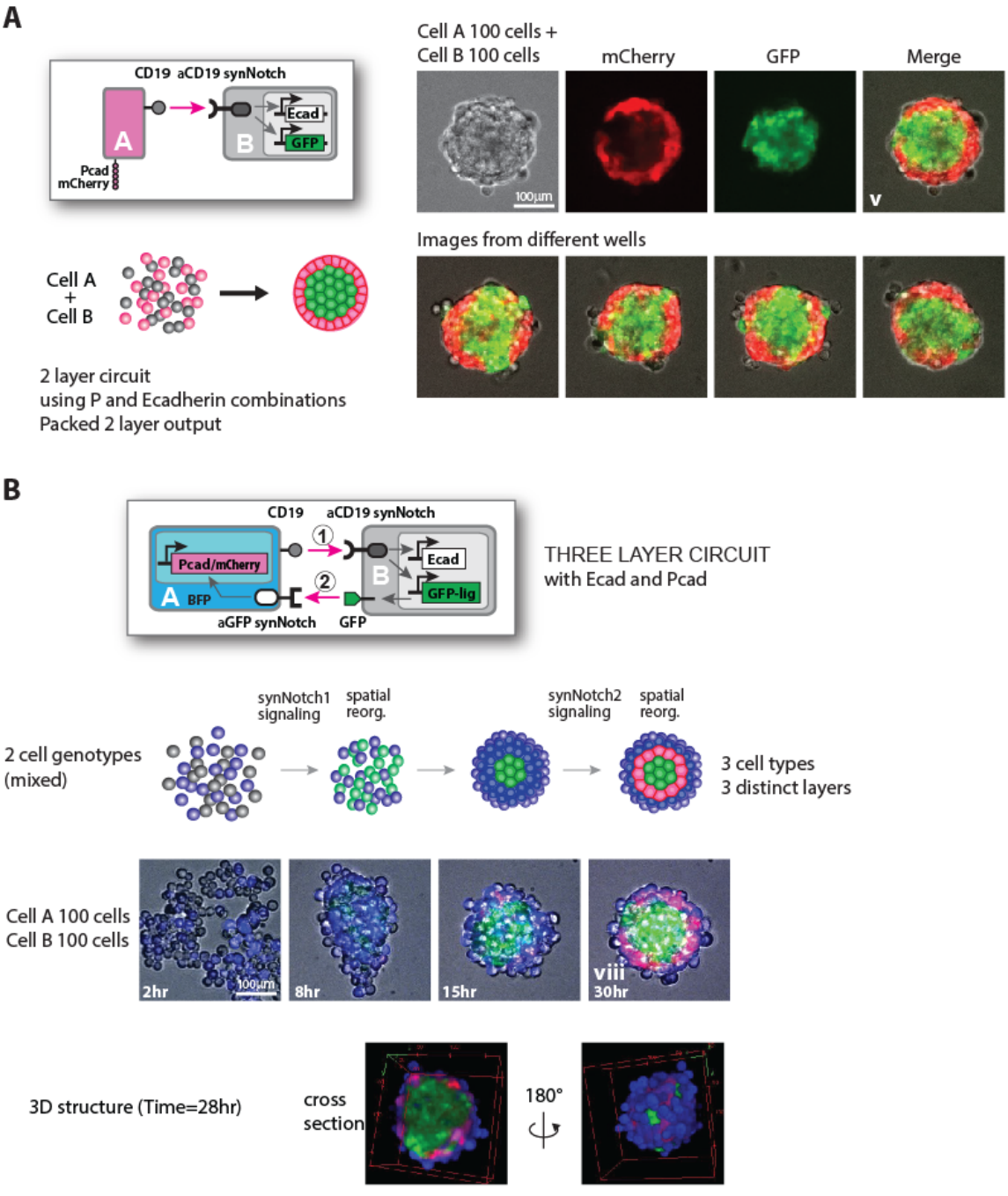

Fig. S9. Spherically symmetric three-layer formation with three-layer circuit inducing Ecadherin and Pcadherin.

(A) Two-layer circuit with Ecad and Pcad. A-type sender cell expressing Pcad and CD19 ligand induces Ecad and GFP in B-type receiver cell via synNotch signaling. When we co-cultured the A-type and B-type cells, Ecad and GFP were induced in B-type cells, leading to two-layer formation of Ecad-positive green core and Pcad-positive red outer layer. The two-layer structure was confirmed with other replicate wells and is also consistent with previous report (12).

(B) Three-layer circuit with Ecad and Pcad. We tested a combination of Ecad and Pcad in the basic three-layer circuit in Fig. 2. A-type cell induces Ecad and GFPlig in B-type cell by CD19 ligand, and then induced GFPlig on B-type cells activates A-type cells to induce Pcad and mCherry. Similarly to the three layer formation with Ecadhi and Ecadlo in Fig. 2, symmetric three layer structure emerged step-wisely with first induction of the green cells, sorting to form an inner core and formation of a red middle layer. 3D reconstruction images starting from 100 A-type cells and 100 B-type cells at 28hr were shown. See Movie S6 for timelapse video and 3D reconstruction.

Supplementary figure 10. Symmetric three-layer formation in a tightly-compacted aggregate.

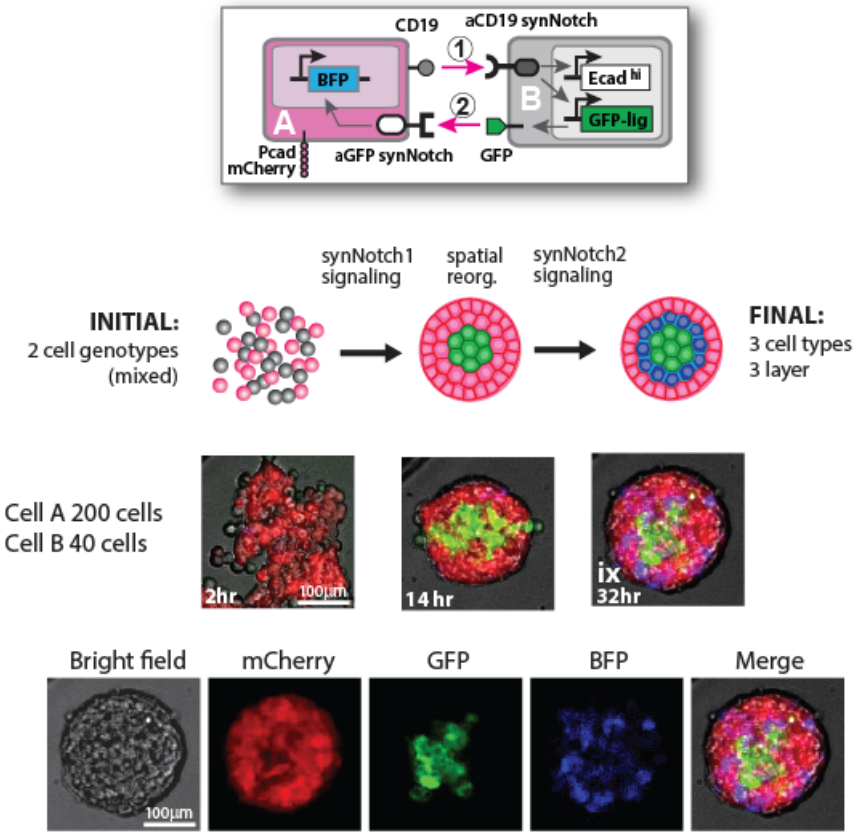

Fig. S10. Symmetric three-layer formation in a tightly-compacted aggregate.

We designed the three-layer circuit inducing Ecad and Pcad in a different sequential manner from Fig. S9B. Pcad-expressing A-type cells induced Ecad and GFPlig in B-type cells, leading to the two-layer formation with B-type cells' green core and A-type cells' red outer layer. Then, A-type cells attaching B-type cells were activated to turn on BFP. Finally, three layer of green Ecad-positive inner core, red Pcad-positive outer layer and blue Pcad-positive boundary region was formed. In this case, differently from symmetric three layer shown in Fig. 2 and Fig. S9B, the outer layer is also tightly compacted thanks to Pcad expression. Images of the three-layer development from 2 to 32hrs and each channel of the final structure were shown. See Movie S7 for timelapse video.

Table S1. Summary table of structures and circuits

No.	structure	Figure	Movie	circuit
i	2 cell types, no spatial org.	Fig. S1a		[Cell A: CD19; CellTrace dye] --> [Cell B: α CD19 synNotch --> GFP]
ii	2 cell types, no spatial org.	Fig. S5b		[Cell A: α CD19 synNotch --> GFP + tTS --| CD19 + mCherry]
iii	2 layer	Fig. 2a-c, S1a		[Cell A: CD19; BFP] --> [Cell B: α CD19 synNotch --> $Ecad_{hi}$ + GFP]
iv	2 layer	Fig. 4, S5	Movie S3	[Cell A: α CD19 synNotch --> Ecad + GFP + tTS --| CD19 + mCherry]
v	2 layer	Fig. S9a		[Cell A: CD19; Pcad; mCherry] --> [Cell B: α CD19 synNotch --> $Ecad_{hi}$ + GFP]
vi	2 layer, asymmetric	Fig. S6b		[Cell A: CD19; Pcad; mCherry] --> [Cell B: α CD19 synNotch --> Ncad + GFP_{lig}]
vii	3 layer	Fig. 2d-f, S2	Movie S1	[Cell A: CD19; BFP; α GFP synNotch] --> [Cell B: α CD19 synNotch --> $Ecad_{hi}$ + GFP_{lig}] --> [Cell A: α GFP synNotch --> $Ecad_{lo}$ + mCherry]
viii	3 layer	Fig. S9b	Movie S6	[Cell A: CD19; BFP; α GFP synNotch] --> [Cell B: aCD19 synNotch --> $Ecad_{hi}$ + GFP_{lig}] --> [Cell A: α GFP synNotch --> Pcad + mCherry]
ix	3 layer	Fig. S10	Movie S7	[Cell A: CD19; Pcad; mCherry; α GFP synNotch] --> [Cell B: α CD19 synNotch --> $Ecad_{hi}$ + GFP_{lig}] --> [Cell A: α GFP synNotch --> BFP]
x	3 layer, asymmetric	Fig. 5b, S7	Movie S4	[Cell A: CD19; BFP; α GFP synNotch] --> [Cell B: α CD19 synNotch --> Ncad + GFP_{lig}] --> [Cell A: α GFP synNotch --> Pcad + mCherry]
xi	3 layer, asymmetric	Fig. 5b, S7	Movie S4	[Cell A: CD19; BFP; α GFP synNotch] --> [Cell B: α CD19 synNotch --> Ncad + GFP_{lig}] --> [Cell A: α GFP synNotch --> Pcad + mCherry]
xii	3 layer, asymmetric	Fig. 5c, S8	Movie S5	[Cell A: CD19; Pcad; mCherry; α GFP synNotch] --> [Cell B: α CD19 synNotch --> Ncad + GFP_{lig}] --> [Cell A: α GFP synNotch --> BFP]

Movie S1. Timelapse videos of three-layer formation and 3D reconstruction image of three-layer structure.

Timelapse videos starting with the co-culture of 200 A-type cells and 40 B-type in the three-layer circuit in Fig. 2D (15x magnification at 30 min/frame from 0hr to 20hr after plating cells) and 160 A-type cells and 80 B-type cells (20x magnification at 15 min/frame from 2hr to 25hr after plating cells). The left window shows a merge of all channels and the right window shows a merge of GFP and mCherry induced by synNotch signaling. 3D reconstruction image of the three-layer structure starting with the co-culture of 200 A-type cells and 40 B-type cells corresponds to the image in Fig.3B.

Movie S2. Bisection of three-layer spheroid with the microfluidic guillotine.

Timelapse video of a three-layer spheroid being cut by the microfluidic guillotine. This video was recorded with high speed camera (Phantom v7.3) mounted on an inverted microscope with a 5× objective. This movie corresponds to the snapshot shown in Fig. 3C.

Movie S3. Timelapse video of two-layer formation from single genotype population.

Timelapse video starting with 100 mCherry-high cells sorted after DAPT treatment in the single genotype two-layer circuit in Fig. 4D. This video was taken with 10x magnification at 30 min/frame from 1hr to 50hr after plating cells. The left window shows a merge of all channels and the right window shows GFP channel induced by the lateral inhibition circuit.

Movie S4. Timelapse videos of asymmetric multi or single-pole three-layer formation and 3D reconstruction of polarized three-layer structure.

Timelapse videos starting with the co-culture of 100 A-type cells and 100 B-type cells, and 30 A-type cells and 30 B-type cells in the three-layer asymmetric circuit (I) in Fig. 5B. This video was taken with 15x magnification at 15 min/frame from 2hr to 50hr after plating cells. The left window shows a merge of all channels and the right window shows a merge of GFP and mCherry induced by synNotch signaling. 3D reconstruction image of the asymmetric single-pole three-layer structure starting with the co-culture of 30 A-type cells and 30 B-type cells corresponds to the image in Fig. S7.

Movie S5. Timelapse video of asymmetric three-layer formation with phase separation and boundary layer activation and 3D reconstruction of its structure.

Timelapse video starting with the co-culture of 160 A-type cells and 80 B-type cells in the three-layer asymmetric circuit (II) in Fig. 5C. This video was taken with 15x magnification at 15 min/frame from 1hr to 34hr after plating cells. The left window shows a merge of all channels and the right window shows a merge of GFP and BFP induced by synNotch signaling. 3D

reconstruction image of the asymmetric three-layer structure starting with the co-culture of 160 A-type cells and 80 B-type cells corresponds to the image in Fig. S8.

Movie S6. Timelapse vide of three-layer formation with Ecad and Pcad and 3D reconstruction of its structure

Timelapse videos starting with the co-culture of 100 A-type cells and 100 B-type cells in the three-layer circuit with Ecad and Pcad in Fig. S9B. This video was taken with 15x magnification at 15 min/frame from 2hr to 30hr after plating cells. The left window shows a merge of all channels and the right window shows a merge of GFP and mCherry induced by synNotch signaling. 3D reconstruction image of the three-layer structure starting with the co-culture of 100 A-type cells and 100 B-type cells corresponds to the image in Fig. S9B.

Movie S7. Timelapse video of three-layer formation in a tight spheroid with Ecad and Pcad

Timelapse video starting with the co-culture of 200 A-type cells and 40 B-type cells in the three-layer circuit with Ecad and Pcad in Fig. S10. This video was taken with 15x magnification at 15 min/frame from 2hr to 32hr after plating cells. The left window shows a merge of all channels and the right window shows a merge of GFP and BFP induced by synNotch signaling.

References and Notes

1. J. Davies, Using synthetic biology to explore principles of development. *Development* **144**, 1146–1158 (2017). doi:10.1242/dev.144196 Medline

2. M. Elowitz, W. A. Lim, Build life to understand it. *Nature* **468**, 889–890 (2010). doi:10.1038/468889a Medline

3. B. P. Teague, P. Guye, R. Weiss, Synthetic morphogenesis. *Cold Spring Harb. Perspect. Biol.* **8**, a023929 (2016). doi:10.1101/cshperspect.a023929 Medline

4. A. Kicheva, N. C. Rivron, Creating to understand - developmental biology meets engineering in Paris. *Development* **144**, 733–736 (2017). doi:10.1242/dev.144915 Medline

5. S. Basu, Y. Gerchman, C. H. Collins, F. H. Arnold, R. Weiss, A synthetic multicellular system for programmed pattern formation. *Nature* **434**, 1130–1134 (2005). doi:10.1038/nature03461 Medline

6. S. S. Jang, K. T. Oishi, R. G. Egbert, E. Klavins, Specification and simulation of synthetic multicelled behaviors. *ACS Synth. Biol.* **1**, 365–374 (2012). doi:10.1021/sb300034m Medline

7. M. Rubenstein, A. Cornejo, R. Nagpal, Robotics. Programmable self-assembly in a thousand-robot swarm. *Science* **345**, 795–799 (2014). doi:10.1126/science.1254295 Medline

8. L. Wolpert, Positional information and the spatial pattern of cellular differentiation. *J. Theor. Biol.* **25**, 1–47 (1969). doi:10.1016/S0022-5193(69)80016-0 Medline

9. D. Gilmour, M. Rembold, M. Leptin, From morphogen to morphogenesis and back. *Nature* **541**, 311–320 (2017). doi:10.1038/nature21348 Medline

10. L. Morsut, K. T. Roybal, X. Xiong, R. M. Gordley, S. M. Coyle, M. Thomson, W. A. Lim, Engineering Customized Cell Sensing and Response Behaviors Using Synthetic Notch Receptors. *Cell* **164**, 780–791 (2016). doi:10.1016/j.cell.2016.01.012 Medline

11. A. Nose, A. Nagafuchi, M. Takeichi, Expressed recombinant cadherins mediate cell sorting in model systems. *Cell* **54**, 993–1001 (1988). doi:10.1016/0092-8674(88)90114-6 Medline

12. D. Duguay, R. A. Foty, M. S. Steinberg, Cadherin-mediated cell adhesion and tissue segregation: Qualitative and quantitative determinants. *Dev. Biol.* **253**, 309–323 (2003). doi:10.1016/S0012-1606(02)00016-7 Medline

13. R. A. Foty, M. S. Steinberg, The differential adhesion hypothesis: A direct evaluation. *Dev. Biol.* **278**, 255–263 (2005). doi:10.1016/j.ydbio.2004.11.012 Medline

14. M. Vinci, S. Gowan, F. Boxall, L. Patterson, M. Zimmermann, W. Court, C. Lomas, M. Mendiola, D. Hardisson, S. A. Eccles, Advances in establishment and analysis of three-dimensional tumor spheroid-based functional assays for target validation and drug evaluation. *BMC Biol.* **10**, 29 (2012). doi:10.1186/1741-7007-10-29 Medline

15. C. Chazaud, Y. Yamanaka, Lineage specification in the mouse preimplantation embryo. *Development* **143**, 1063–1074 (2016). doi:10.1242/dev.128314 Medline

16. S. E. Harrison, B. Sozen, N. Christodoulou, C. Kyprianou, M. Zernicka-Goetz, Assembly of embryonic and extraembryonic stem cells to mimic embryogenesis in vitro. *Science* **356**, eaal1810 (2017). doi:10.1126/science.aal1810 Medline

17. A. Sánchez Alvarado, P. A. Tsonis, Bridging the regeneration gap: Genetic insights from diverse animal models. *Nat. Rev. Genet.* **7**, 873–884 (2006). doi:10.1038/nrg1923 Medline

18. L. R. Blauch, Y. Gai, J. W. Khor, P. Sood, W. F. Marshall, S. K. Y. Tang, Microfluidic guillotine for single-cell wound repair studies. *Proc. Natl. Acad. Sci. U.S.A.* **114**, 7283–7288 (2017). doi:10.1073/pnas.1705059114 Medline

19. J. R. Collier, N. A. M. Monk, P. K. Maini, J. H. Lewis, Pattern formation by lateral inhibition with feedback: A mathematical model of delta-notch intercellular signalling. *J. Theor. Biol.* **183**, 429–446 (1996). doi:10.1006/jtbi.1996.0233 Medline

20. S. J. Bray, Notch signalling: A simple pathway becomes complex. *Nat. Rev. Mol. Cell Biol.* **7**, 678–689 (2006). doi:10.1038/nrm2009 Medline

21. M. Matsuda, M. Koga, K. Woltjen, E. Nishida, M. Ebisuya, Synthetic lateral inhibition governs cell-type bifurcation with robust ratios. *Nat. Commun.* **6**, 6195 (2015). doi:10.1038/ncomms7195 Medline

22. S. Wennekamp, S. Mesecke, F. Nédélec, T. Hiiragi, A self-organization framework for symmetry breaking in the mammalian embryo. *Nat. Rev. Mol. Cell Biol.* **14**, 452–459 (2013). doi:10.1038/nrm3602 Medline

23. S. C. van den Brink, P. Baillie-Johnson, T. Balayo, A.-K. Hadjantonakis, S. Nowotschin, D. A. Turner, A. Martinez Arias, Symmetry breaking, germ layer specification and axial organisation in aggregates of mouse embryonic stem cells. *Development* **141**, 4231–4242 (2014). doi:10.1242/dev.113001 Medline

24. J. Vendome, K. Felsovalyi, H. Song, Z. Yang, X. Jin, J. Brasch, O. J. Harrison, G. Ahlsen, F. Bahna, A. Kaczynska, P. S. Katsamba, D. Edmond, W. L. Hubbell, L. Shapiro, B. Honig, Structural and energetic determinants of adhesive binding specificity in type I cadherins. *Proc. Natl. Acad. Sci. U.S.A.* **111**, E4175–E4184 (2014). doi:10.1073/pnas.1416737111 Medline

25. E. Cachat, W. Liu, K. C. Martin, X. Yuan, H. Yin, P. Hohenstein, J. A. Davies, 2- and 3-dimensional synthetic large-scale de novo patterning by mammalian cells through phase separation. *Sci. Rep.* **6**, 20664 (2016). doi:10.1038/srep20664 Medline

26. A. M. Turing, The chemical basis of morphogenesis. *Philos. Trans. R. Soc. Lond. B Biol. Sci.* **237**, 37–72 (1952). doi:10.1098/rstb.1952.0012

27. M. D. Jacobson, M. Weil, M. C. Raff, Programmed cell death in animal development. *Cell* **88**, 347–354 (1997). doi:10.1016/S0092-8674(00)81873-5 Medline

28. E. Scarpa, R. Mayor, Collective cell migration in development. *J. Cell Biol.* **212**, 143–155 (2016). doi:10.1083/jcb.201508047 Medline

29. E. Li, Chromatin modification and epigenetic reprogramming in mammalian development. *Nat. Rev. Genet.* **3**, 662–673 (2002). doi:10.1038/nrg887 Medline

30. J. A. Davies, Synthetic morphology: Prospects for engineered, self-constructing anatomies. *J. Anat.* **212**, 707–719 (2008). doi:10.1111/j.1469-7580.2008.00896.x Medline

31. S. A. Newman, R. Bhat, Dynamical patterning modules: A "pattern language" for development and evolution of multicellular form. *Int. J. Dev. Biol.* **53**, 693–705 (2009). doi:10.1387/ijdb.072481sn Medline

32. Y. E. Antebi, N. Nandagopal, M. B. Elowitz, An operational view of intercellular signaling pathways. *Curr. Opin. Syst. Biol.* **1**, 16–24 (2017). doi:10.1016/j.coisb.2016.12.003 Medline

33. J. B. A. Green, J. Sharpe, Positional information and reaction-diffusion: Two big ideas in developmental biology combine. *Development* **142**, 1203–1211 (2015). doi:10.1242/dev.114991 Medline

34. Y. Hart, S. Reich-Zeliger, Y. E. Antebi, I. Zaretsky, A. E. Mayo, U. Alon, N. Friedman, Paradoxical signaling by a secreted molecule leads to homeostasis of cell levels. *Cell* **158**, 1022–1032 (2014). doi:10.1016/j.cell.2014.07.033 Medline

35. Y. Okabe, R. Medzhitov, Tissue biology perspective on macrophages. *Nat. Immunol.* **17**, 9–17 (2016). doi:10.1038/ni.3320 Medline

36. N. King, M. J. Westbrook, S. L. Young, A. Kuo, M. Abedin, J. Chapman, S. Fairclough, U. Hellsten, Y. Isogai, I. Letunic, M. Marr, D. Pincus, N. Putnam, A. Rokas, K. J. Wright, R. Zuzow, W. Dirks, M. Good, D. Goodstein, D. Lemons, W. Li, J. B. Lyons, A. Morris, S. Nichols, D. J. Richter, A. Salamov, J. G. I. Sequencing, P. Bork, W. A. Lim, G. Manning, W. T. Miller, W. McGinnis, H. Shapiro, R. Tjian, I. V. Grigoriev, D. Rokhsar, The genome of the choanoflagellate Monosiga brevicollis and the origin of metazoans. *Nature* **451**, 783–788 (2008). doi:10.1038/nature06617 Medline

37. M. Abedin, N. King, The premetazoan ancestry of cadherins. *Science* **319**, 946–948 (2008). doi:10.1126/science.1151084 Medline

38. S. A. Nichols, B. W. Roberts, D. J. Richter, S. R. Fairclough, N. King, Origin of metazoan cadherin diversity and the antiquity of the classical cadherin/β-catenin complex. *Proc. Natl. Acad. Sci. U.S.A.* **109**, 13046–13051 (2012). doi:10.1073/pnas.1120685109 Medline

39. R. A. Alegado, L. W. Brown, S. Cao, R. K. Dermenjian, R. Zuzow, S. R. Fairclough, J. Clardy, N. King, A bacterial sulfonolipid triggers multicellular development in the closest living relatives of animals. *eLife* **1**, e00013 (2012). doi:10.7554/eLife.00013 Medline

40. A. Woznica *et al.*, Bacterial lipids activate, synergize, and inhibit a developmental switch in choanoflagellates. *Proc. Natl. Acad. Sci.* **113**, 7894–7899 (2016).

41. S. A. Grupp, M. Kalos, D. Barrett, R. Aplenc, D. L. Porter, S. R. Rheingold, D. T. Teachey, A. Chew, B. Hauck, J. F. Wright, M. C. Milone, B. L. Levine, C. H. June, Chimeric antigen receptor-modified T cells for acute lymphoid leukemia. *N. Engl. J. Med.* **368**, 1509–1518 (2013). doi:10.1056/NEJMoa1215134 Medline

42. P. C. Fridy, Y. Li, S. Keegan, M. K. Thompson, I. Nudelman, J. F. Scheid, M. Oeffinger, M. C. Nussenzweig, D. Fenyö, B. T. Chait, M. P. Rout, A robust pipeline for rapid production of versatile nanobody repertoires. *Nat. Methods* **11**, 1253–1260 (2014). doi:10.1038/nmeth.3170 Medline